Palaeogeography, Palaeoclimatology, Palaeoecology 518 (2019) 206–214

Contents lists available at ScienceDirect

Palaeogeography, Palaeoclimatology, Palaeoecology

journal homepage: www.elsevier.com/locate/palaeo

Asynchronous Holocene Climate Optimum across mid-latitude Asia

Fuyuan Gao[a,b], Jia Jia[b,*], Dunsheng Xia[b], Caichen Lu[b], Hao Lu[b], Youjun Wang[b], Hao Liu[b], Yapeng Ma[b], Kaiming Li[a]

[a] College of Geography and Environmental Engineering, Lanzhou City University, Lanzhou 730070, China
[b] MOE Key Laboratory of West China's Environmental System, College of Earth and Environmental Sciences, Lanzhou University, Lanzhou 730000, China

ARTICLE INFO

Keywords:
Holocene Climate Optimum
Moisture
Spatiotemporal
Chinese Loess Plateau
Xinjiang
Tajikistan

ABSTRACT

The Holocene Climate Optimum (HCO) was an important interval in the development of human civilization and has been the focus of many paleoclimatic studies. However, there are significant regional differences in the timing of the HCO due to the complex response of regional climates to insolation changes, associated with internal feedbacks within the climate system. Here, we present the results of a study of magnetic and geochemical properties of loess-paleosol sequences from across mid-latitude Asia, with the aim of assessing differences in the timing of the HCO. The HCO generally occurred after ~5 ka in Tajikistan and Xinjiang; during 5–2.5 ka in the western Chinese Loess Plateau (CLP); and during ~8–2.5 ka in the central CLP. This asynchroneity reflects differences in the response of regional climates to global climate change. Specifically, the difference in timing between the central and western CLP may have been related to shifts in the position of the East Asian summer monsoon rain belt, due to the changing longitudinal position of the Western Pacific Subtropical High, together with changes in the east-west thermal gradient in the equatorial Pacific (i.e. shifts between La Niña and El Niño conditions).

1. Introduction

The Holocene Climate Optimum (HCO) in China is defined as a humidity maximum (An et al., 2000). The spatiotemporal pattern of the HCO has become a focus of Holocene climate research in mid-latitude Asia (e.g. He et al., 2004; Li et al., 2015), yet its characteristics are controversial. One viewpoint, based on the oxygen isotope record of stalagmites, is that the HCO was synchronous across mid-latitude Asia, with a moisture maximum during ~10–5 ka (Cheng et al., 2012). By contrast, lake sediment records indicate an asynchronous HCO between the regions respectively dominated by the westerlies and the East Asian summer monsoon (EASM). The stalagmite record has the significant advantage of high precision U-series dating, and its $\delta^{18}O$ record is considered a reliable precipitation proxy (Wang et al., 2001, 2005, 2008; Yuan et al., 2004; Cheng et al., 2005). However, recent research has highlighted that various factors can control the variations of stalagmite $\delta^{18}O$ in China, such as the "circulation effect" (Pausata et al., 2011; Yang et al., 2014; Liu et al., 2015; Tan, 2009, 2011, 2014; Tan and Nan, 2010; Caley et al., 2014) and vapor source (Clemens et al., 2010). Pollen records from lake sediments are regarded as a reliable climate proxy and have been widely used for reconstructing past climate change (An et al., 2012; Wang et al., 2013; Jiang et al., 2013; Chen et al., 2015). The influence of the "reservoir effect" on ^{14}C dates of bulk lake sediment samples remains an unresolved problem for dating both organic and inorganic carbon. Although several approaches to assessing the magnitude of the "reservoir effect" have been developed (Hou et al., 2012; Zhang et al., 2016), the problem may significantly affect the reliability of estimates of the timing of the HCO based on lake sediments.

Eolian loess is a major climatic archive and has provided a wealth of information on regional climatic change during the Quaternary (e.g. Porter, 2001; Ding et al., 2002a). In mid-latitude Asia, Holocene loess is characterized by a wide distribution and quasi-continuous deposition. The time resolution of the loess deposits of the Tienshan Mountains (Chen et al., 2016) and the Chinese Loess Plateau (CLP) (Xia et al., 2014; Huang et al., 2006) are ~35–100 y/cm and 28–55 y/cm, respectively, and thus they can be used to study millennial-scale climate change. Previous paleoclimatic studies of loess have focused mainly on the central CLP (Huang et al., 2006; Jia et al., 2008), and the broad, arid and semi-arid region of loess deposition from the western CLP to central Asia remains poorly documented. In the present study, we compare magnetic and geochemical records of Holocene loess sequences in the East Asian monsoon-dominated region (the central and western CLP) and the westerlies-dominated region (Tajikistan and

* Corresponding author.
E-mail address: jiaj@zjnu.edu.cn (J. Jia).

https://doi.org/10.1016/j.palaeo.2019.01.012
Received 27 February 2018; Received in revised form 9 January 2019; Accepted 10 January 2019
Available online 14 January 2019
0031-0182/ © 2019 Elsevier B.V. All rights reserved.

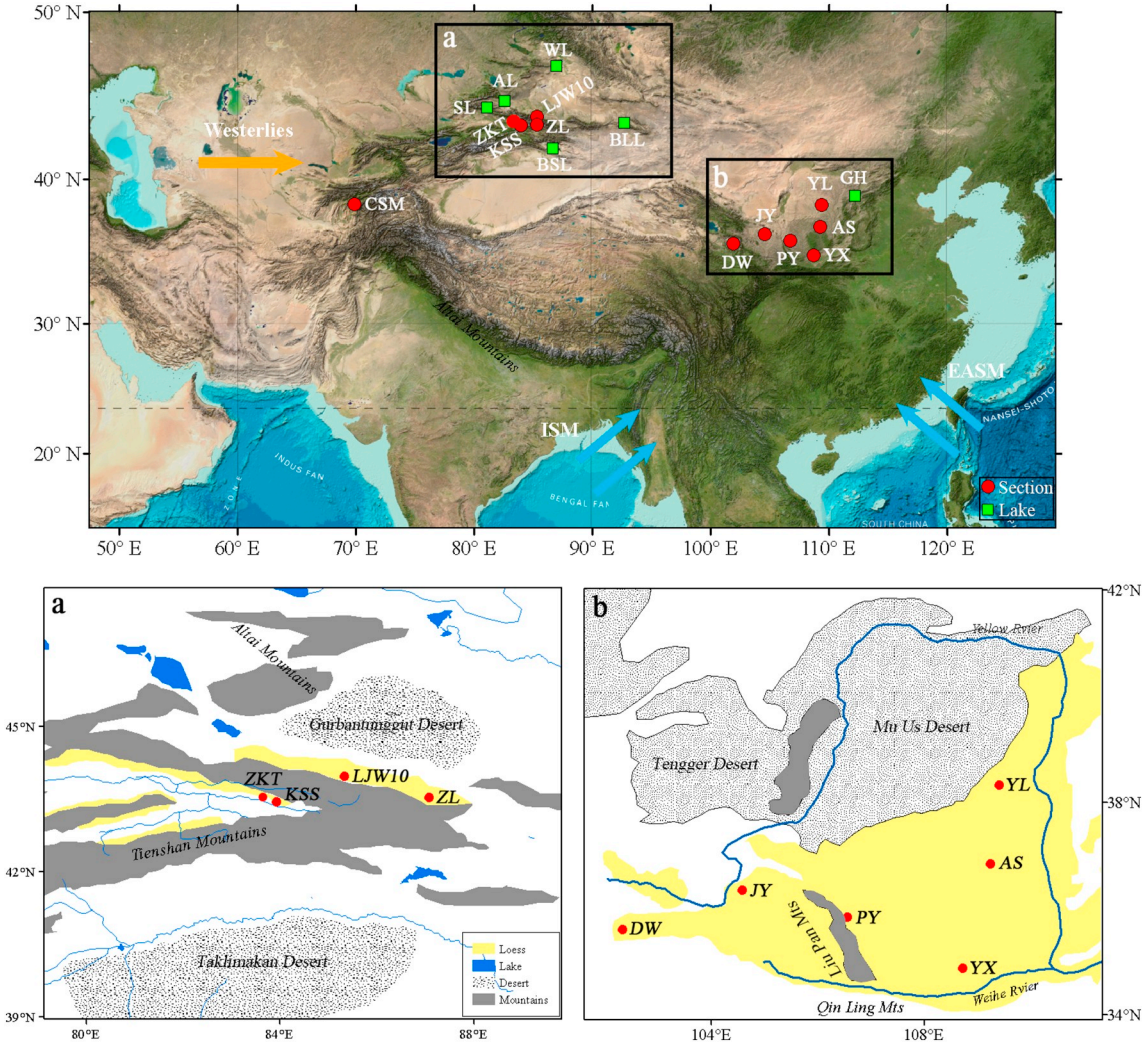

Fig. 1. Location of the study area and study sections. EASM: East Asian summer monsoon. ISM: Indian summer monsoon. YL: Yulin section (Lu et al., 2013); AS: Ansai section; YX: Yaoxian section (Xia et al., 2014); PY: Pengyang section; JY: Jingyuan section (Sun et al., 2010); DW: Duowa section (Maher and Hu, 2006); LJW10: Lujiaowan10 section (Chen et al., 2016); ZL: Zhongliang section (Chen et al., 2016); KSS: Kansu section (Chen et al., 2016); ZKT: Zeketai section (Feng et al., 2011); CSM: CSM section; GH: Gonghai lake (Chen et al., 2015); BLL: Balikun lake (An et al., 2012); BSL: Bosten lake (Huang et al., 2009); WL: Wulungu lake (Yang and Wang, 1996); AL: Aibi lake (Wang et al., 2013); SL: Sayram lake (Jiang et al., 2013).

Xinjiang). With the aim was to investigating the spatiotemporal pattern of the HCO in mid-latitude Asia.

2. Study area and sections

2.1. Study area

The CLP, in central China, is divided into three geographical regions by the Liupan and Lvliang Mountains (Fig. 1; Liu, 1985). The climate of the CLP is dominated by the East Asian monsoon circulation. In summer, the East Asian summer monsoon (EASM) carries warm and moist air masses to the CLP; this causes heavy rainfall, which is concentrated from July to September, and promotes strong soil development. In winter, the climate is dominated by the East Asian winter monsoon (EAWM), which carries cold, dry air masses to the CLP and transports large amounts of eolian dust (Dong et al., 2015). From southeast to northwest across the CLP, the average annual rainfall decreases from 600–700 mm to 100–200 mm (Yu et al., 2002).

Xinjiang is the most important area of loess accumulation in central Asia, and loess deposits are widespread across parts of the northern Kunlun Mountains, the Yili River valley, and the northern Tienshan Mountains (Sun, 2002). The Junggar Basin contains widespread desert and Gobi deposits and has an arid climate. The following sequence of vegetation zones occurs with increasing altitude from the arid basin to the mountains: desert, desert steppe, mountain steppe, mountain forest, alpine meadow, mountain desert, ice and bare rock. In the arid basin, the mean annual temperature (MAT) ranges from 3 to 5 °C in the northern part and 5–7.5 °C in the southern part. The mean annual precipitation (MAP) is less than 150 mm across most of the region. With increasing altitude from the basin to the northern Tienshan Mountains, at ~2000 m above sea level, the MAT decreases and the MAP increases to ~500 mm The Yili River valley is relatively humid, with MAP ranging from 200 to 500 mm on the plains and increasing to 800 mm in the mountains (Ye, 1999). MAT varies from 2.6 to 9.2 °C, depending on altitude. The vegetation exhibits a strong altitudinal gradient and the following zones occur with increasing altitude: desert, montane steppe, montane forest-meadow, subalpine meadow, alpine meadow, and alpine cushion-like vegetation (Xinjiang Expedition Team of CAS, 1979).

Tajikistan, bordered by Xinjiang Province to the east, is a major area of loess deposition in central Asia (Ding et al., 2002b). Present-day moisture transport to Tajikistan occurs mainly via the westerlies from the Atlantic Ocean, the Mediterranean and the Caspian Sea, together with local recycling. Winter precipitation is a prevailing feature in central Asia (Cheng et al., 2016). The climate of Tajikistan is

continental, subtropical and semiarid and changes rapidly with elevation. The average temperature range is 23–30 °C in July and −1 to 3 °C in January at lower elevations, whereas in the eastern Pamirs it is 5–10 °C in July and −15 °C to −20 °C in January. Most of Tajikistan has a MAP of 700–1600 mm, with the heaviest precipitation occurring at the Fedchenko Glacier and the lightest in the eastern Pamirs (Li et al., 2016).

2.2. Study sections

2.2.1. Loess sections in the central CLP

Three loess sections were investigated in the central CLP: Yulin (YL; 38°20′N, 109°44′E) (Lu et al., 2013), Yaoxian (YX; 34°53′N, 108°45′E) (Xia et al., 2014), and Ansai (AS; 36°51′N, 109°16′E). Detailed lithological and dating descriptions of the YL and YX sections are given in Lu et al. (2013) and Xia et al. (2014), respectively. For the present study, two new samples from the YX section were chosen for AMS ^{14}C dating. A previously undocumented AS section is in northern Shanxi Province (Fig. 1). The section is 2.65-m thick and the lithology is as follows: 0–0.3 m - modern soil; 0.3–0.9 m - loess; 0.9–2.1 m - paleosol; 2.1–2.35 m - calcic horizon; 2.35–2.65 m - loess. Four samples for AMS ^{14}C dating were collected, and the sampling interval for environmental proxies was 5 cm.

2.2.2. Loess sections in the western CLP

Three loess sections were reviewed and investigated in the area. Details of the lithology and dating of the Duowa section (DW; 35°25′N, 101°57′E) are given in Maher and Hu (2006), and those for the Jingyuan section (JY; 30°23′N, 104°37′E) are given in Sun et al. (2010). For the present study, new samples of the JY section were collected at 2-cm intervals for environmental proxy measurements. The PY section (35°52′27″N, 106°44′04″E) is a new section located in the Liupan Mountains (Fig.1). The section is 2.3-m-thick and the lithology is as follows: 0–0.3 m - modern soil; 0.3–0.6 m - loess; 0.6–1.7 m - paleosol; 1.7–2.3 m - loess. Four samples for AMS ^{14}C dating were collected, and the sampling interval for environmental proxies was 5 cm.

2.2.3. Loess sections in Xinjiang

Four loess sections were reviewed in the Xinjiang area. The Lujiaowan section (LJW10; 43°58′29″N, 85°20′10″E) and Zhongliang section (ZL; 43°30′16″N, 85°20′19″E) are on the northern slopes of the Northern Tienshan Mountains. The Kansu section (KSS; 43°26′42″N, 83°55′39″E) and Zeketai section (ZKT; 43°32′13″N , 83°18′51″E) are in the Yili River valley. Detailed lithological descriptions of these sections are given in Chen et al. (2016).

2.2.4. Loess sections in Tajikistan

The CSM section (38°23′32″N, 69°49′57″E) is in southern Tajikistan. The section is 1.6-m - thick and the lithology is as follows: 0–0.4 m - paleosol; 0.4–0.7 m - loess; 0.7–1.1 m - calcic horizon; 1.1–1.6 m - loess. Four samples for AMS ^{14}C dating were collected and the sampling interval for environmental proxies was 2 cm (Table 1).

Table 1
The studied loess sections.

	Study sections	Reference
Central CLP	Yulin (YL)	Lu et al., 2013
	Yaoxian (YX)	Xia et al., 2014
	Ansai (AS)	This study
West CLP	Jingyuan (JY)	Sun et al., 2010
	Duowa (DW)	Maher and Hu, 2006
	Pengyang (PY)	This study
Central Asia	Lujiaowan10 (LJW10)	Chen et al., 2016
	Zhongliang (ZL)	Chen et al., 2016
	Kansu (KS)	Chen et al., 2016
	Zeketai (ZKT)	Chen et al., 2016
	CSM	This study

3. Methods

3.1. Sediment dating

Some of the AMS ^{14}C dates for the KSS and ZL sections are given in Chen et al. (2016). In this study, 13 samples of bulk organic matter from the KSS, ZL, AS and PY sections were chosen for AMS ^{14}C dating. Graphite samples were prepared in the Chronology Laboratory of Lanzhou University using direct CO_2 catalytic reduction of iron powder, as described by Vogel et al. (1987) and Hatté et al. (2001). The samples were analyzed in the AMS ^{14}C Dating Laboratory of Beijing University (PKUAMS, Beijing, China) using the pretreatment procedures described by Goh and Molloy (1978). In addition, 7 samples of bulk organic matter for AMS ^{14}C dating were collected from the YX, AS and CSM sections and measured by Beta Analytic, U.S.A. All dates were calibrated to calendar years before 1950 CE based on the INTCAL04 dataset (Reimer et al., 2004) using the program CALIB 7.02 (Table 2). For the ZKT section, 17 radiocarbon dates from snail carbonate have been published (Feng et al., 2011).

Chronological data for the LJW10 section were provided by Li et al. (2015), who conducted quartz OSL dating of the coarse-grained (63–90 μm) fraction, and applied K-feldspar pIRIR dating protocols to both the coarse-grained (63–90 μm) and medium-grained (38–63 μm) fractions. Three OSL dates were reported by Xia et al. (2014) for the YX section and four dates by Sun et al. (2010) for the JY section. Continuous time series were established for each section using curve fitting based on the AMS ^{14}C and OSL dates (Fig. 2).

3.2. Magnetic measurements

After air-drying in the laboratory, weighed samples were packed into 2 × 2 × 2 cm^3 plastic boxes and used for measurements of low-frequency (470 Hz) and high-frequency (4700 Hz) magnetic susceptibility (χ_{lf} and χ_{hf}, respectively) using a Bartington Instruments MS2B magnetic susceptibility meter. The two measurements were used to calculate the frequency-dependence of magnetic susceptibility (χ_{fd}), defined as χ_{lf}-χ_{hf}.

3.3. Geochemical measurements

Samples for the measurement of element concentrations were selected at a 5-cm interval from the AS and PY sections, at a 10-cm interval for the KSS section, and at a 4-cm interval for the CSM section. Bulk samples were ground to pass through a 200-mesh (75 μm) sieve. Subsequently, ~4 g of sediment was placed in a mold with boric acid on the edge and base, and disc-shaped samples (32-mm diameter) were produced using a pressure of 30 t. Element concentrations were measured using a Philips PW2403 X-Ray Fluorescence (XRF) spectrometer. The measurement precision of XRF is 0.1%–0.3%.

4. Interpretation of climate proxies

The χ_{lf} values of loess samples are usually controlled by the content of strongly magnetic minerals, such as magnetite and maghemite, which may be of lithogenic and pedogenic origin. The content of pedogenic magnetite and maghemite is strongly correlated with soil moisture content and its seasonal variation (Maher, 1998). In humid seasons (high soil moisture content), Fe ion is separated from non-magnetic or weakly magnetic minerals by soil organic acids, in response to a reduction in soil redox potential. Thus, the Fe ion must be in the reduced form. In arid seasons (low soil moisture content), the redox potential is enhanced and ferrous ions are gradually oxidized to ferric ions. Both ions can then be utilized in chemical reactions to form magnetite and maghemite (Chen et al., 2016). Where the concentration

Table 2
Results of AMS ^{14}C dating of the studied sections.

Sample	Depth (m)	Material	Methods	^{14}C age (a BP)	Calendar age (cal. a BP)
YX-137[a]	1.37–1.38	Bulk organic matter	AMS 14C	2820 ± 30	2925 ± 36
YX-399[a]	3.99–4.00	Bulk organic matter	AMS 14C	13,430 ± 40	16,385 ± 408
AS-60[b]	0.55–0.60	Bulk organic matter	AMS 14C	2210 ± 25	2231 ± 161
AS-135[b]	1.30–1.35	Bulk organic matter	AMS 14C	4045 ± 30	4513 ± 160
AS-210[b]	2.05–2.10	Bulk organic matter	AMS 14C	6695 ± 35	7569 ± 126
AS-265[a]	2.60-2.65	Bulk organic matter	AMS 14C	8610 ± 30	9560 ± 20
PY-55[b]	0.50–0.55	Bulk organic matter	AMS 14C	1550 ± 20	1457 ± 43
PY-120[b]	1.15–1.20	Bulk organic matter	AMS 14C	3765 ± 25	4144 ± 42
PY-170[b]	1.65–1.70	Bulk organic matter	AMS 14C	5025 ± 30	5796 ± 69
PY-230[b]	2.25–2.30	Bulk organic matter	AMS 14C	5560 ± 25	6354 ± 34
ZL-40[b]	0.40–0.50	Bulk organic matter	AMS 14C	5040 ± 40	5806 ± 67
ZL-110[b]	1.10–1.20	Bulk organic matter	AMS 14C	8170 ± 60	9143 ± 91
ZL-140[b]	1.40–1.50	Bulk organic matter	AMS 14C	9400 ± 810	10,820 ± 1113
KSS-10[b]	0.10–0.20	Bulk organic matter	AMS 14C	460 ± 40	512 ± 18
KSS-40[b]	0.40–0.50	Bulk organic matter	AMS 14C	1800 ± 40	1731 ± 67
KSS-70[b]	0.70–0.80	Bulk organic matter	AMS 14C	3125 ± 45	3341 ± 54
CSM-10[a]	0.10-0.12	Bulk organic matter	AMS 14C	190 ± 30	154 ± 124
CSM-20[a]	0.20–0.22	Bulk organic matter	AMS 14C	1040 ± 30	956 ± 18
CSM-50[a]	0.50–0.52	Bulk organic matter	AMS 14C	1870 ± 30	1809 ± 49
CSM-80[a]	0.80–0.82	Bulk organic matter	AMS 14C	5330 ± 30	6108 ± 67

[a] Beta Analytic, USA.
[b] Samples prepared in the Chronology Laboratory of Lanzhou University and analyzed in the AMS ^{14}C Dating Laboratory of Beijing University.

of lithogenic magnetic minerals is low and stable, the variations in χ_{lf} values are controlled by the amount of pedogenic magnetite and maghemite. This relationship means that χ_{lf} can be used to recover paleoclimatic information from loess sequences. However, if the concentration of lithogenic magnetic minerals is high and variable, the interpretation of the χ_{lf} record is complex and it may not be possible to use it recover paleoclimatic information. In the CLP, the loess-paleosol sequences exhibit strong pedogenesis. The signal of lithogenic magnetic minerals is completely dominated by that of pedogenic magnetic minerals, and therefore χ_{lf} is commonly used as an indicator of pedogenesis and summer monsoon moisture (Chen et al., 1999). Loess-paleosol sequences in some areas of Xinjiang exhibit weak pedogenesis because of the dry climate, resulting in very low concentrations of the pedogenic magnetic fraction (Zan et al., 2010), which may thus be obscured by the signal of lithogenic magnetic minerals. In this case, therefore, χ_{lf} cannot be used as an indicator of pedogenesis (e.g. Wei et al., 2013). However, at relatively high altitudes, as precipitation increase, soil development is intensified; thus, in the case of well-developed soils at high altitudes, χ_{lf} can be used as an indicator of pedogenesis (e.g. Jia et al., 2018). In summary, χ_{lf} cannot universally be used as a proxy of pedogenic intensity in Xinjiang.

The magnetic characteristics of the lithological component of loess deposits are typically dominated by coarse-grained ferrimagnetic materials, such as pseudo-single domain (PSD) and multidomain (MD) magnetite. By contrast, the magnetic characteristics of the pedogenic component of loess are typically dominated by fine-grained

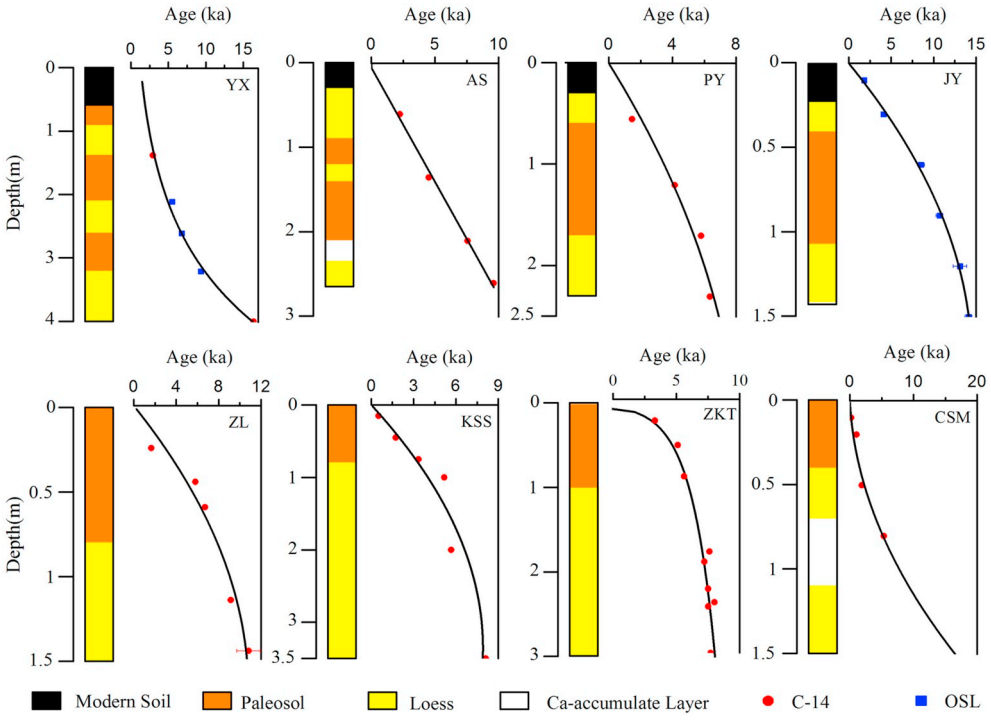

Fig. 2. Lithology and ages of sections YX, AS, PY, JY, ZL, KSS, ZKT and CSM.

ferrimagnets such as SP and SSD magnetite and maghemite (Nie et al., 2013). χ_{fd} is particularly sensitive to the concentration of SP ferrimagnetic grains (Thompson and Oldfield, 1986). Where the content of fine-grained pedogenic ferrimagnets is high, χ_{fd} can be used as a paleoclimatic proxy. However, in very dry environments such as in some deserts, where the concentration of pedogenic fine-grained ferrimagnets is low, χ_{fd} cannot be used as a paleoclimatic indicator. A study of modern processes demonstrated that the χ_{fd} of topsoil in the Tienshan Mountains and the CLP is closely related to the MAP (Guo et al., 2011); this indicated that χ_{fd} could be used as paleoclimatic proxy, both in the CLP and the Tienshan Mountains. χ_{ARM} is particularly sensitive to the concentration of SSD ferrimagnetic grains and SIRM reflects the total content of remanence-bearing minerals (Thompson and Oldfield, 1986). The χ_{ARM}/SIRM ratio is a useful index of the representation of fine ferrimagnetic grains in magnetic mineral assemblages. A high content of fine-grained pedogenic ferrimagnets would lead to high values of χ_{ARM}/SIRM, indicating strong pedogenesis. Therefore, χ_{ARM}/SIRM can be used as an indicator of pedogenic intensity, and has been used for this purpose in loess deposits, especially in areas of weak pedogenesis (Li et al., 2015; Zhao et al., 2016; Chen et al., 2016).

The weathering of rocks is an important source of mineral elements for ecosystems and is a key process in soil development (Song, 2006). Strong weathering is a prerequisite for soil formation and a warm, humid climate promotes strong weathering. Therefore, weathering intensity has been used to reconstruct paleoclimatic changes recorded in lake and eolian sediments (Jin et al., 2006; Chen et al., 2003). In this study, we used the Rb/Sr ratio and the $(CaO + Na_2O + K_2O)/Al_2O_3$ ration as proxies for the weathering intensity of eolian sediments. In eolian sediments, Rb tends to be dispersed in K-bearing minerals such as K-feldspar, muscovite and some clay minerals, whereas Sr is associated with Ca-bearing minerals such as plagioclase and carbonates. Weathering effects dominate the variations in Rb/Sr in eolian sediments. During strong chemical weathering, Sr-bearing minerals are more susceptible to decomposition than Rb-bearing minerals; this results in Sr depletion from the soil while Rb is retained, thus increasing the Rb/Sr ratio (Chen et al., 2003). Therefore, variations in the Rb/Sr ratio of eolian sediments are related to weathering intensity.

Based on the foregoing, we selected χ_{lf}, χ_{fd} and Rb/Sr ratio for use as moisture proxies on the CLP, and χ_{ARM}/SIRM, χ_{fd} and Rb/Sr ratio as moisture proxies for Xinjiang and Tajikistan.

5. Results

5.1. East Asian monsoon region

5.1.1. Central CLP

The magnetic parameters for the YL, YX and AS sections exhibit a similar pattern, with low values occurring before ~8 ka and after ~2.5 ka, and high values occurring during ~8–2.5 ka. The Rb/Sr ratio of the AS section is also high during ~8–2.5 ka (Figs. 3a–c, 4a). These characteristics are consistent with the stratigraphy which consists of loess layers before ~8 ka and after ~2.5 ka, and paleosol layers during ~8–2.5 ka. These characteristics suggest that in the central CLP the HCO occurred during ~8–2.5 ka.

5.1.2. Western CLP

The values of all the magnetic parameters of the DW, JY and PY sections are higher during ~5–2.5 ka than before ~5 ka and after ~2.5 ka. The variation of the Rb/Sr ratio for the PY section also exhibits a maximum during ~5–2.5 ka. These characteristics indicate that in the western CLP the HCO occurred during ~5–2.5 ka (Figs. 3d–f, 4b).

5.2. Central Asia

5.2.1. Xinjiang

The record of χ_{ARM}/SIRM and χ_{fd} for the LJW10, ZL, ZKT and KSS

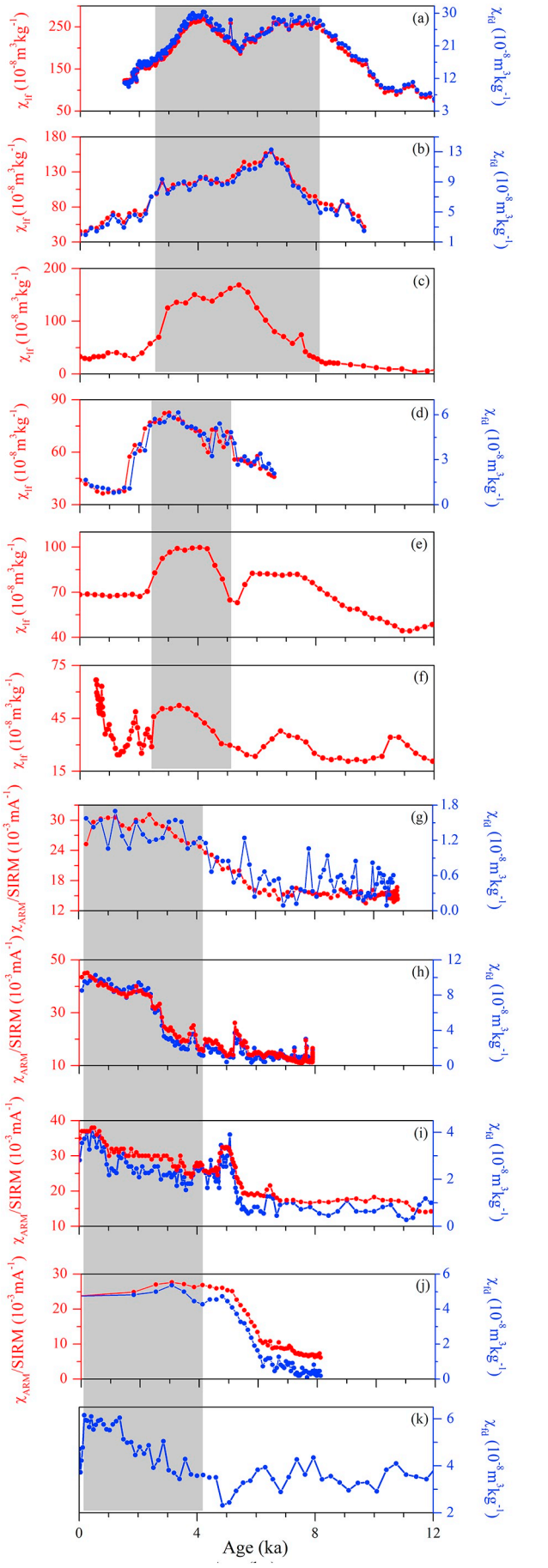

(caption on next page)

Fig. 3. Comparison of the timing of the Holocene Climatic Optimum for sites from Tajikistan, Xinjiang, west CLP and central CLP. a: YL; b: AS; c: YX; d: PY; e: JY; f: DW; g: LJW10; h: ZL; i: KSS; j: ZKT; k: CSM.

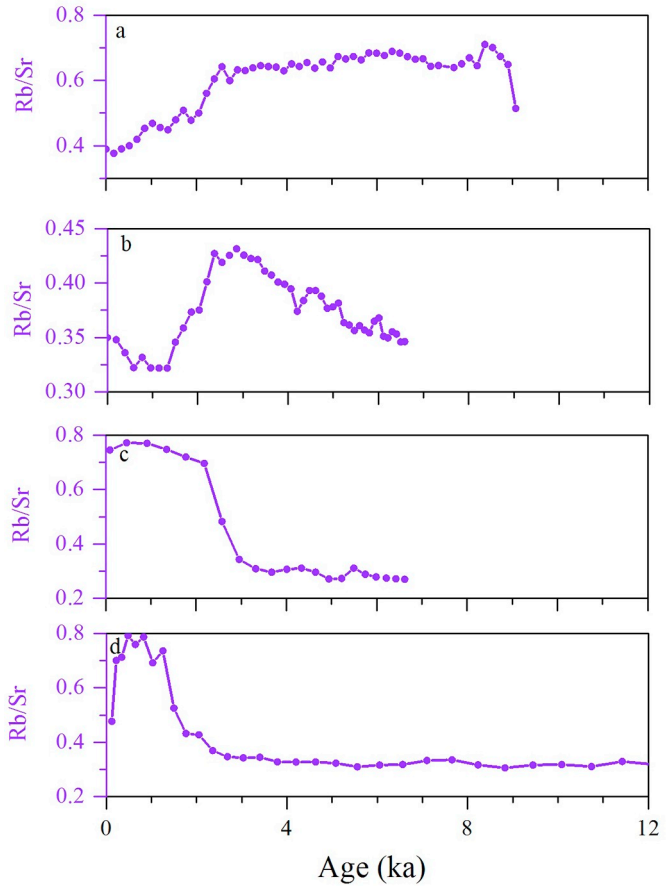

Fig. 4. Rb/Sr ratios for sections AS (a), PY (b), KSS (c) and CSM (d).

sections, and the Rb/Sr record for the KSS section, indicate a gradual enhancement of pedogenic development and weathering from the mid Holocene. This indicates that in Xinjiang the HCO occurred in the late Holocene (after ~5 ka) (Figs. 3g-j, 4c).

5.2.2. Tajikistan

The four loess sections in Xinjiang are located on the eastern fringe of central Asia, where the rainfall season occurs in summer rather than in winter, as is typical of most of ACA. This leads to uncertainty regarding whether the Holocene climate records for the Xinjiang area are representative of the whole of central Asia (Cheng et al., 2016). Therefore, one new loess section (CSM) in southern Tajikistan was also investigated. The AMS ^{14}C chronology and profiles of χ_{fd} and Rb/Sr ratio indicate that the area experienced a similar pattern of climate change to that of the Xinjiang area, with dry conditions in the early-middle Holocene and relatively moist conditions in the late Holocene. Thus, in Tajikistan the HCO occurred in the late Holocene (Figs. 3k, 4d).

6. Discussion

6.1. Time-transgressive nature of the HCO at the study sites

The variation of the Rb/Sr ratio and magnetic parameters from the loess sections in the central CLP, west CLP and central Asia exhibit different patterns. Relatively humid conditions occurred from ~8–7 to ~2.5 ka in the central CLP, during ~5–2.5 ka in the western CLP, and after ~5 ka in central Asia.

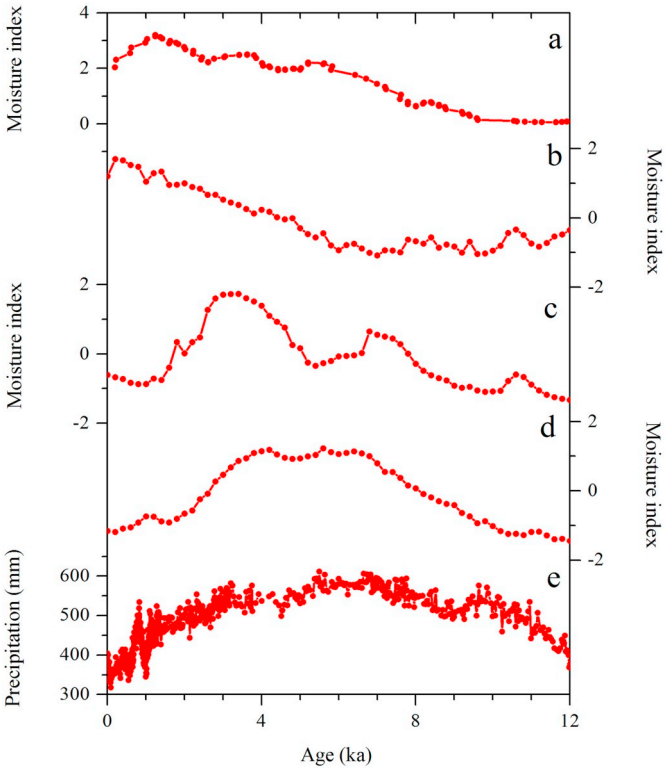

Fig. 5. Comparison of magnetic and other moisture/precipitation records from central Asia and North China. a: Standardized moisture records for the Xinjiang region (Wang et al., 2013). b: Standardized χ_{ARM}/SRIM record for the Tajikistan and Xinjiang loess sections. c: Standardized χ_{lf} record for the western CLP. d: Standardized χ_{lf} record for the central CLP. e: Pollen-based quantitative annual precipitation record from GH (Chen et al., 2015).

To further compare the humidity records of these sections, the χ_{lf} records from the central CLP (YL, AS, YX), western CLP (PY, JY, DW) and central Asia (LJW10, KSS, ZL, CSM) were standardized and averaged. This was accomplished as follows: continuous time series were generated by using curve fitting based on the AMS ^{14}C and OSL dates, and each 200-year interval was assigned a χ_{lf} value (for the CLP) or χ_{ARM}/SIRM value (for central Asia). The data were then standardized using the regularization approach, calculated as $Z = (x - \mu) / \sigma$, where Z is the standard score, and μ and σ are the arithmetic mean and standard deviation, respectively. Finally, the regional average value was calculated from the standardized data for the individual sections (Fig. 5).

As shown in Fig. 5d, the HCO occurred during ~8–2.5 ka in the central CLP. A recent high-resolution, pollen-based quantitative reconstruction of mean annual precipitation from Gonghai Lake, in the eastern CLP, revealed a relatively humid mid-Holocene (8–3 ka) with precipitation peaking during 7–5 ka (Fig. 5e; Chen et al., 2015). Pollen records from the Hani peatland (Yu et al., 2008), Bayanchagan Lake (Jiang et al., 2006) and Daihai Lake (Xiao et al., 2004) also revealed a mid-Holocene moisture maximum. In addition, Wang et al. (2010), in an evaluation of the Holocene evolution of the EASM, suggested that the EASM precipitation maximum occurred during 7–4 ka.

As shown in Fig. 5c, in the western CLP the HCO occurred during ~5–2.5 ka. The region exhibits an overall similar pattern of moisture evolution to the central CLP (Fig. 5d), but with two significant differences: the HCO occurred later and was of shorter duration in the western CLP than in the central CLP.

As shown in Fig. 5b, our results show that in central Asia, moisture increased from ~5 ka and that the HCO occurred in the late Holocene. A pollen record from lake sediments further suggests that humidity

gradually increased from the mid-Holocene in northern Xinjiang (Fig. 5a; Wang et al., 2013), and even in the Caspian Sea region (Leroy et al., 2014). A summer rainfall estimate, based on $\delta^{13}C$ analyses of a site from the Chaiwobu peatland in Xinjiang, indicates an overall increasing trend since 8.5 ka, albeit with several fluctuations (Hong et al., 2014). However, in Xinjiang and the surrounding region, lakes did not develop until the mid-Holocene (Chen et al., 2008). A high-resolution, multi-proxy Holocene climate record from Lake Urmia (NW Iran) indicates that the coolest and driest conditions occurred during 10.3–7.0 ka; cool and dry episodes occurred during 7.0–3.5 ka; and warm and wet conditions occurred during 3.0–0.5 ka (Haghipour et al., 2016). In addition, simulated annual precipitation in central Asia increased continuously during the Holocene (Chen et al., 2016). These various lines of evidence all indicate that in the westerlies-dominated region, the HCO occurred in the late Holocene.

In summary, the HCO occurred earliest in the central CLP, followed by the western CLP, and then by central Asia (Figs. 3 and 5). This finding is supported by a comprehensive study combining various proxy records and climate model results which also suggested that the Holocene summer precipitation/moisture maximum occurred later in Xinjiang, the northwestern Loess Plateau and western Inner Mongolia, compared to the monsoon region (Jin et al., 2014).

6.2. Possible mechanisms for the asynchronous precipitation maximum

The paleoclimate proxy records for central Asia indicate a relatively humid climate in the late Holocene due to persistently increasing summer and winter precipitation. This was mainly caused by the strengthening of the westerlies, increasing winter insolation and the southward displacement of the subtropical high. The insolation gradient between mid- latitudes and high-latitudes can be regarded as a temperature gradient which can be used to as a proxy of the westerlies intensity (Jin et al., 2012). Winter/summer insolation at mid-latitudes increases/decreases faster than at high-latitudes, causing a generally increased insolation gradient (temperature gradient) from the early Holocene onwards, and the increased insolation gradient (temperature gradient) indicates that both the winter and summer westerlies gradually intensified during the Holocene (Chen et al., 2016). In winter, the gradual increase in winter insolation during the Holocene may have supplied more moisture to the strengthening westerlies, therefore bringing more precipitation to central Asia (Wang et al., 2013). In summer, higher temperatures in the early Holocene would have caused the northward displacement of the subtropical high which would have decreased the precipitation in central Asia. With the decreasing temperatures in the late Holocene, the gradual southward displacement of the subtropical high would have resulted in a reduced influence in central Asia, and hence to increased precipitation in that region (Chen et al., 2016).

In the central CLP, the HCO occurred in the mid-Holocene because of changes in Northern Hemisphere summer insolation (NHSI) and Atlantic meridional overturning circulation (AMOC) (Chen et al., 2015). Climate simulation results demonstrate that an anomalous freshening of the North Atlantic and the resulting weakened AMOC could have greatly weakened the insolation-driven EASM through the strengthening of westerly and northerly winds (Chen et al., 2015). This would have caused a weaker EASM during the early Holocene than during the mid-Holocene (Chen et al., 2015).

In the western CLP, the HCO occurred in the mid-late Holocene (~5–2.5 ka), which may be attributed to variations in the position of the Western Pacific Subtropical High (WPSH) and the intensity of the EASM. The northerly and westerly variations in the position of the WPSH have a critical influence on the location of the EASM rain belt. In summer, precipitation (i.e. the EASM rain belt) forms north of the WPSH when warm and moist flow air from the ocean meets cold air flow from the mid-latitude continents. Therefore, the EASM rain belt will extend to the north/west with the northerly/westerly variations in the position of the WPSH. However, the northerly and westerly variations of the position of the WPSH are not entirely synchronous; for example, it was in a relatively northeasterly position during 1968–1978 (EASM strong years) and in a relatively southwesterly position during 1979–1998 (EASM weak years) (Qian et al., 2007; Tan, 2009). A previous study found that an overall La Niña status was accompanied by a more northward- and eastward- located WPSH (Tan and Nan, 2010). An enhanced west-east thermal gradient in the equatorial Pacific (La Niña) during the mid-Holocene (Koutavas and Joanides, 2012; Fig. 6a), implies that the WPSH may have retreated eastwards during 8–5 ka. Climate models indicate an eastward extension of the WPSH before 5 ka and a westward extension subsequently (Wang et al., 2015). Climate records from lake sediments and peat deposits indicate a weaker EASM during the early Holocene (~8 ka), a stronger EASM during the mid-late Holocene (~8–3 ka, Fig. 6b), and a weakened EASM in the late Holocene (~3–0 ka) (Xiao et al., 2004; Jiang et al., 2006; Yu et al., 2008; Wang et al., 2010; Chen et al., 2015). Integrating the information derived from variations in the intensity of the EASM and the location of the WPSH leads us to propose the following scenario: 1) *Early Holocene* (before ~8 ka). The weak EASM resulted in low precipitation in both the central and western CLP (Fig. 6c and d). 2) *Mid-Holocene* (~8–5 ka BP). A stronger EASM was accompanied by a gradual eastward shift in the WPSH, enabling the EASM rain belt to reach the central CLP and resulting in significantly increased precipitation (Fig. 6c). However, the EASM rain belt may not have reached the western CLP where precipitation remained low (Fig. 6d). 3) *Mid-late Holocene* (~5–3 ka). The westward extension of the WPSH and stronger EASM led to a westward expansion of the rain belt, which not only reached the central CLP but also the western CLP. Precipitation thus remained high in the central CLP and increased in the western CLP (Fig. 6c and d). 4) *Late Holocene* (~3–0 ka). Despite the westward extension of the WPSH, precipitation decreased in both the central and western CLP due to the rapidly weakening EASM, in response to decreasing summer insolation (Fig. 6c and d).

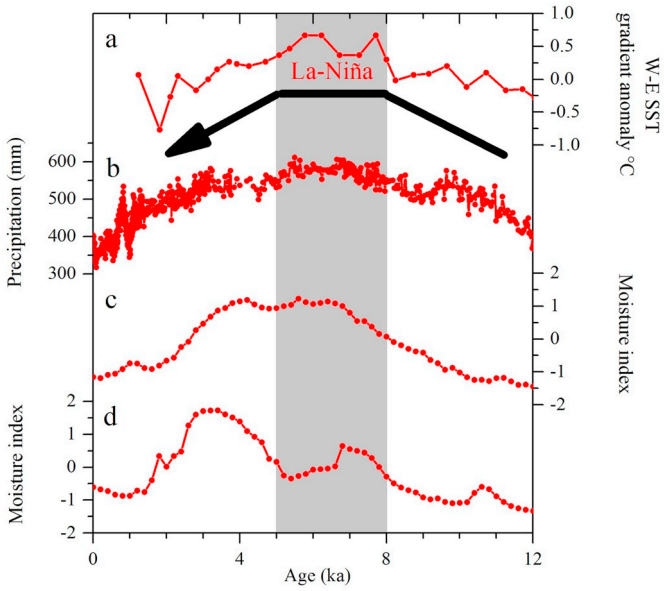

Fig. 6. a, Record of the west-east thermal gradient in the equatorial Pacific (Koutavas and Joanides, 2012); b, pollen-based quantitative annual precipitation record from core GH (Chen et al., 2015); c, the moisture evolution of central CLP; d, the moisture evolution of the western CLP.

7. Conclusions

We have investigated and reviewed a series of Holocene loess-paleosol sequences in mid-latitude Asia, including sites in the central CLP,

western CLP, Xinjiang and Tajikistan. Using magnetic properties and selected element concentrations as rainfall proxies, we conclude that the HCO occurred earliest in the central CLP, followed by the western CLP, and then by central Asia. The difference in the timing of the HCO between the CLP and central Asia can be attributed to the operation of regional climate systems. Specifically, the difference between the central and western CLP may have resulted from the changing position of the EASM rain belt due to changes in the longitudinal position of the western WPSH, accompanied by shifts in the west-east thermal gradient in the equatorial Pacific (i.e. changes between La Niña and El Niño conditions).

Acknowledgements

This work was supported by the National Key R&D Program of China (Grant 2018YFA0606401), the Natural Science Foundation of China (Grant No. 41401046) and International Partnership Program of Chinese Academy of Sciences (Grant No. 131C11KYSB20160061). We thank Dr. Jan Bloemendal for critical discussions, constructive suggestions and English improvement.

References

An, Z., Porter, S.C., Kutzbach, J.E., Wu, X., Wang, S., Liu, X., Li, X., Zhou, W., 2000. Asynchronous Holocene optimum of the East Asia monsoon. Quat. Sci. Rev. 19, 743–762.

An, C.B., Lu, Y.B., Zhao, J.J., Tao, S.C., Dong, W.M., Li, H., Jin, M., Wang, Z.L., 2012. A high-resolution record of Holocene environmental and climatic changes from Lake Balikun (Xinjiang, China): implications for central Asia. The Holocene 22, 43–52.

Caley, T., Roche, D.M., Renssen, H., 2014. Orbital Asian summer monsoon dynamics revealed using an isotope-enabled global climate model. Nat. Commun. 5, 5371.

Chen, F.H., Bloemendal, J., Feng, Z.D., Wang, J.M., Parker, E., Guo, Z.T., 1999. East Asian monsoon variations during oxygen isotope stage 5: evidence from the northwestern margin of the Chinese loess plateau. Quat. Sci. Rev. 18, 1127–1135.

Chen, Y., Che, J., Liu, L.W., Ji, J.F., Zhang, J.X., 2003. Spatial and temporal changes of summer monsoon on the Loess Plateau of Central China during the last 130 ka inferred from Rb/Sr ratios. Sci. China Ser. D Earth Sci. 46, 1022–1030.

Chen, F.H., Yu, Z.C., Yang, M.L., Ito, E., Wang, S.M., Madsen, D.B., Huang, X.Z., Zhao, Y., Sato, T., Birks, H.J.B., Boomer, I., Chen, J.H., An, C.B., Wünnemann, B., 2008. Holocene moisture evolution in arid central Asia and its out-of-phase relationship with Asian monsoon history. Quat. Sci. Rev. 27, 351–364.

Chen, F.H., Xu, Q.H., Chen, J.H., Birks, H.J.B., Liu, J.B., Zhang, S.R., Jin, L.Y., An, C.B., Telford, R.J., Cao, X.Y., Wang, Z.L., Zhang, X.J., Selvaraj, K., Lü, H.Y., Li, Y.C., Zheng, Z., Wang, H.P., Zhou, A.F., Dong, G.H., Zhang, J.W., Huang, X.Z., Bloemendal, J., Rao, Z.G., 2015. East Asian summer monsoon precipitation variability since the last deglaciation. Sci. Rep. 5, 11186.

Chen, F.H., Jia, J., Chen, J.H., Li, G.Q., Zhang, X.J., Xie, H.C., Xia, D.S., Huang, W., An, C.B., 2016. A persistent Holocene wetting trend in arid central Asia, with wettest conditions in the late Holocene, revealed by multi-proxy analyses of loess-paleosol sequences in Xinjiang, China. Quat. Sci. Rev. 146, 134–146.

Cheng, H., Edwards, R.L., Wang, X.F., Wang, Y.J., Kong, X.G., Yuan, D.X., Zhang, M.L., Lin, Y.S., Qin, J.M., Ran, J.C., 2005. Oxygen isotope records of stalagmites from Southern China. Quat. Sci. 25, 157–163 (in Chinese with English abstract).

Cheng, H., Zhang, P.Z., SpÖtl, C., Edwards, R.L., Cai, Y.J., Zhang, D.Z., Sang, W.C., Tan, M., An, Z.S., 2012. The climatic cyclicity in semiarid-arid central Asia over the past 500,000 years. Geophys. Res. Lett. 39, L01705.

Cheng, H., Spötl, C., Breitenbach, S.F.M., Sinha, A., Wassenburg, J.A., Jochum, K.P., Scholz, D., Li, X.L., Yi, L., Peng, Y.B., Lv, Y.B., Zhang, P.Z., Votintseva, A., Loginov, V., Ning, Y.F., Kathayat, G., Edwards, L., 2016. Climate variations of central Asia on orbital to millennial timescales. Sci. Rep. 5, 36975.

Clemens, S.C., Prell, W.L., Sun, Y.B., 2010. Orbital-scale timing and mechanisms driving late Pleistocene Indo-Asian summer monsoons: reinterpreting cave speleothem $\delta^{18}O$. Paleoceanography 25, PA4207.

Ding, Z.L., Derbyshire, E., Yang, S.L., Yu, Z.W., Xiong, S.F., Liu, T.S., 2002a. Stacked 2.6-Ma grain size record from the Chinese loess based on five sections and correlation with the deep-sea $\delta^{18}O$ record. Paleoceanography 17 (5-1-5-21).

Ding, Z.L., Ranov, V., Yang, S.L., Finaev, A., Han, J.M., Wang, G.A., 2002b. The loess record in southern Tajikistan and correlation with Chinese loess. Earth Planet. Sci. Lett. 200, 387–400.

Dong, Y., Wu, N., Li, F., Huang, L., Wen, W., 2015. Time-transgressive nature of the magnetic susceptibility record across the Chinese loess plateau at the Pleistocene/Holocene transition. PLoS One 10, e0133541.

Feng, Z.D., Ran, M., Yang, Q.L., Zhai, X.W., Wang, W., Zhang, X.S., Huang, C.Q., 2011. Stratigraphies and chronologies of late Quaternary loess-paleosol sequences in the core area of the Central Asian Arid Zone. Quat. Int. 240, 156–166.

Goh, K.M., Molloy, B.P.J., 1978. Radiocarbon dating of paleosoils using soil organic matter components. J. Soil Sci. 29, 567–573.

Guo, X.L., Liu, X.M., Bin, L.Ü., Tang, D.P., Mao, X.G., Chen, J.S., Chen, C.Y., 2011. Comparison of topsoil magnetic properties between the loess region in Tianshan mountains and loess plateau, China, and its environmental significance. Chin. J. Geophys. 54, 1854–1862.

Haghipour, N., Eglinton, T., Mcintyre, C., Darvishi Khatooni, J., Hunziker, D., Mohammadi, A., 2016. Paleo-climate and paleo-environment reconstruction based on a high-resolution, multi-proxy Holocene lake record from Lake Urmia (NW Iran). In: EGU General Assembly Conference. EGU General Assembly Conference Abstracts, vol. 18.

Hatté, C., Pessenda, L.C., Lang, A., Paterne, M., 2001. Development of accurate and reliable ^{14}C chronologies for loess deposits: application to the loess sequence of nussloch (Rhine valley, Germany). Radiocarbon 43, 611–618.

He, Y., Theakstone, W.H., Zhang, Z., Zhang, D., Yao, T., Chen, T., Shen, Y., Pang, H., 2004. Asynchronous Holocene climatic change across China. Quat. Res. 61, 52–63.

Hong, B., Gasse, F., Uchida, M., Hong, Y., Leng, X., Shibata, Y., An, N., Zhu, Y.X., Wang, Y., 2014. Increasing summer rainfall in arid eastern-central Asia over the past 8500 years. Sci. Rep. 4, 5279.

Hou, J., D'Andrea, W.J., Liu, Z., 2012. The influence of ^{14}C reservoir age on interpretation of paleolimnological records from the Tibetan Plateau. Quat. Sci. Rev. 48, 67–79.

Huang, C.C., Pang, J., Chen, S., Su, H., Han, J., Cao, Y., Zhao, W., Tan, Z., 2006. Charcoal records of fire history in the Holocene loess–soil sequences over the southern loess plateau of China. Palaeogeogr. Palaeoclimatol. Palaeoecol. 239, 28–44.

Huang, X.Z., Chen, F.H., Fan, Y.X., Yang, M.L., 2009. Dry late-glacial and early Holocene climate in arid central Asia indicated by lithological and palynological evidence from Bosten Lake, China. Quat. Int. 194, 19–27.

Jia, Y., Huang, C., Pang, J., Niu, J., 2008. Chronology of the holocene loess-paleosol section and its deposition and pedogenesis on the south of Chinese loess plateau. J. Geogr. Sci. 18, 425–442.

Jia, J., Gao, F.Y., Xia, D.S., Huang, W., Chen, F.H., 2018. Moisture variations in arid central Asia and its out-of-phase relationship with the Asian Monsoon during MIS 5: evidence from loess records. J. Quat. Sci. 33, 435–443.

Jiang, W.Y., Guo, Z.T., Sun, X.J., Wu, H.B., Chu, G.Q., Yuan, B.Y., Hatte, C., Guiot, J., 2006. Reconstruction of climate and vegetation changes of Lake Bayanchagan (Inner Mongolia): Holocene variability of the East Asian monsoon. Quat. Res. 65, 411–420.

Jiang, Q.F., Ji, J.F., Shen, J., Matsumoto, R., Tong, G.B., Qian, P., Ren, X.M., Yan, D.Z., 2013. Holocene vegetational and climatic variation in westerly-dominated areas of Central Asia inferred from the Sayram Lake in northern Xinjiang, China. Sci. China Earth Sci. 56, 339–353.

Jin, Z., Cao, J., Wu, J., Wang, S., 2006. A Rb/Sr record of catchment weathering response to Holocene climate change in Inner Mongolia. Earth Surf. Process. Landf. 31, 285–291.

Jin, L., Chen, F., Morrill, C., Otto-Bliesner, B., Rosenbloom, N., 2012. Causes of early Holocene desertification in arid central Asia. Clim. Dyn. 38, 1577–1591.

Jin, L., Schneider, B., Park, W., Latif, M., Khon, V., Zhang, X., 2014. The spatial-temporal patterns of Asian summer monsoon precipitation in response to Holocene insolation change: a model-data synthesis. Quat. Sci. Rev. 85, 47–62.

Koutavas, A., Joanides, S., 2012. El Niño–Southern Oscillation Extrema in the Holocene and last Glacial Maximum. Paleoceanography 27, PA4208.

Leroy, S.A.G., Lopez-Merino, L., Tudryn, A., Chalie, F., Gasse, F., 2014. Late Pleistocene and Holocene palaeoenvironments in and around the middle Caspian basin as reconstructed from a deep-sea core. Quat. Sci. Rev. 101, 91–110.

Li, G.Q., Wen, L.J., Xia, D.S., Duan, Y.W., Rao, Z.G., Madsen, D.B., Wei, H.T., Li, F.L., Jia, J., Chen, F.H., 2015. Quartz OSL and K-feldspar pirir dating of a loess/paleosol sequence from arid central Asia, Tianshan Mountains, NW China. Quat. Geochronol. 28, 40–53.

Li, Q., Wu, H., Yu, Y., Sun, A., Markovi, S.B., Guo, Z., 2015. Reconstructed moisture evolution of the deserts in northern China since the Last Glacial Maximum and its implications for the East Asian Summer Monsoon. Glob. Planet. Chang. 121, 101–112.

Li, G.H., Xia, D.S., Jia, J., Zhao, S., Gao, F.Y., Wang, Y.J., Lu, H., Chen, F.H., 2015. Magnetic properties derived from a loess section at the northern piedmont of Tianshan Mountains, Xinjiang, China, and their paleoenvironmental significance. Geophys. J. Int. 203, 828–839.

Li, Y., Song, Y., Chen, X., Li, J., Mamadjanov, Y., Aminov, J., 2016. Geochemical composition of Tajikistan loess and its provenance implications. Palaeogeogr. Palaeoclimatol. Palaeoecol. 446, 186–194.

Liu, T.S., 1985. Loess and the Environment. China Ocean Press, Beijing.

Liu, J.B., Chen, J.H., Zhang, X.J., Li, Y., Rao, Z.G., Chen, F.H., 2015. Holocene East Asian summer monsoon records in northern China and their inconsistency with Chinese stalagmite $\delta^{18}O$ records. Earth Sci. Rev 148, 194–208.

Lu, H.Y., Yi, S.W., Liu, Z.Y., Mason, J.A., Jiang, D.B., Cheng, J., Stevens, T., Xu, Z.W., Zhang, E.L., Jin, L.Y., Zhang, Z.H., Guo, Z.T., Wang, Y., Otto-Bliesner, B., 2013. Variation of East Asian monsoon precipitation during the past 21 ky and potential CO_2 forcing. Geology 41, 1023–1026.

Maher, B.A., 1998. Magnetic properties of modern soils and Quaternary loessic paleosol: paleoclimatic implication. Palaeogeogr. Palaeoclimatol. Palaeoecol 137, 25–54.

Maher, B.A., Hu, M., 2006. A high-resolution record of Holocene rainfall variations from the western Chinese Loess Plateau: antiphase behaviour of the African/Indian and East Asian summer monsoons. The Holocene 16, 68–76.

Nie, J.S., Song, Y.G., King, J.W., Zhang, R., Fang, X.M., 2013. Six million years of magnetic grain-size records reveal that temperature and precipitation were decoupled on the Chinese loess plateau during ~ 4.5-2.6 ma. Quat. Res 79, 465–470.

Pausata, F.S.R., Battisti, D.S., Nisancioglu, K.H., Bitz, C.M., 2011. Chinese stalagmite $\delta^{18}O$ controlled by changes in the Indian monsoon during a simulated Heinrich event. Nat. Geosci. 4, 474–480.

Porter, S.C., 2001. Chinese loess record of monsoon climate during the last glacial interglacial cycle. Earth Sci. Rev. 54, 115–128.

Qian, W., Lin, X., Zhu, Y., Xu, Y., Fu, J., 2007. Climatic regime shift and decadal

anomalous events in China. Clim. Chang. 84, 167–189.
Reimer, P.J., Baillie, M.G.L., Bard, E., Bayliss, A., Beck, J.W., Blackwell, P.G., Buck, C.E., Burr, G.S., Cutler, K.B., Damon, P.E., Edwards, R.L., Fairbanks, R.G., Friedrich, M., Guilderson, T.P., Hogg, A.G., Hughen, K.A., Kromer, B., McCormac, G., Manning, S., Ramsey, C.B., Reimer, R.W., Remmele, S., Southon, J.R., Stuiver, M., Talamo, S., Taylor, F.W., van der Plicht, J., Weyhenmeyer, C.E., 2004. IntCal04 Terrestrial radiocarbon age calibration, 0–26 cal kyr BP. Radiocarbon 46, 1029–1058.
Song, Z.L., 2006. The Weathering and Pedogenesis Effect and Its Mineral Elements Behavior and Environmental Quality in Karst Watershed. Graduate University of the Chinese Academy of Sciences, Beijing (in Chinese with English abstract).
Sun, J.M., 2002. Source regions and formation of the loess sediments on the high mountain regions of Northwestern China. Quat. Res. 58, 341–351.
Sun, Y., Wang, X., Liu, Q., Clemens, S.C., 2010. Impacts of post-depositional processes on rapid monsoon signals recorded by the last glacial loess deposits of northern China. Earth Planet. Sci. Lett. 289, 171–179.
Tan, M., 2009. Circulation effect: climatic significance of the short term variability of the oxygen isotopes in stalagmites from monsoonal China-dialogue between paleoclimate records and modern climate research. Quat. Sci. 29, 851–861 (in Chinese with English abstract).
Tan, M., 2011. Trade-wind driven inverse coupling between stalagmite $\delta^{18}O$ from monsoon region of China and large scale temperature-circulation effect on decadal to precessional timescales. Quat. Sci. 31, 1086–1097 (in Chinese with English abstract).
Tan, M., 2014. Circulation effect: response of precipitation $\delta^{18}O$ to the ENSO cycle in monsoon regions of China. Clim. Dyn. 42, 1067–1077.
Tan, M., Nan, S.L., 2010. Primary investigation on interannual changes in the circulation effect of precipitation oxygen isotopes in monsoon China. Quat. Sci. 30, 620–622 (in Chinese with English abstract).
Thompson, R., Oldfield, F., 1986. Environmental Magnetism. Allen & Unwin, London.
Vogel, J.S., Southon, J.R., Nelson, D.E., 1987. Catalyst and binder effects in the use of filamentous graphite for AMS. Nucl. Instrum. Methods Phys. Res. 29, 50–56.
Wang, Y.J., Cheng, H., Edwards, R.L., An, Z.S., Wu, J.Y., Shen, C.C., Dorale, J.A., 2001. A high resolution absolute-dated late Pleistocene monsoon record from Hulu Cave, China. Science 294, 2345–2348.
Wang, Y.J., Cheng, H., Edwards, R.L., He, Y.Q., Kong, X.G., An, Z.S., Wu, J.Y., Kelly, M.J., Dykoski, C.A., Li, X.D., 2005. The Holocene Asian Monsoon: links to solar changes and North Atlantic climate. Science 308, 854–857.
Wang, Y.J., Cheng, H., Edwards, R.L., Kong, X.G., Shao, X.H., Chen, S.T., Wu, J.Y., Jiang, X.Y., Wang, X.F., An, Z.S., 2008. Millennial-and orbital-scale changes in the East Asian monsoon over the past 224,000 years. Nature 451, 1090–1093.
Wang, Y., Liu, X., Herzschuh, U., 2010. Asynchronous evolution of the Indian and East Asian Summer Monsoon indicated by Holocene moisture patterns in monsoonal central Asia. Earth Sci. Rev. 103, 135–153.
Wang, W., Feng, Z.D., Ran, M., Zhang, C.J., 2013. Holocene climate and vegetation changes inferred from pollen records of Lake Aibi, northern Xinjiang, China: a potential contribution to understanding of Holocene climate pattern in East-central Asia. Quat. Int. 311, 54–62.
Wang, N., Zhang, X.J., Jin, L.Y., 2015. The spatial and temporal variation characteristics of the South Asia high and Western Pacific Subtropical High on millennial time. Quat. Sci. 36, 1425–1436 (in Chinese with English abstract).
Wei, H.T., Banerjee, S.K., Xia, D.S., Jackson, M.J., Jia, J., Chen, F.H., 2013. Magnetic characteristics of loess-paleosol sequences on the north slope of the Tianshan Mountains, northwestern China and their paleoclimatic implications. Chin. J. Geophys. 56, 150–158 (in Chines with English abstract).
Xia, D., Jia, J., Li, G., Zhao, S., Wei, H., Chen, F., 2014. Out-of-phase evolution between summer and winter east Asian monsoons during the Holocene as recorded by Chinese loess deposits. Quat. Res. 81, 500–507.
Xinjiang Expedition Team of CAS, 1979. The vegetation and its utilization in Xinjiang. Science Press, Beijing.
Xiao, J., Xu, Q., Nakamura, T., Yang, X., Liang, W., Inouchi, Y., 2004. Holocene vegetation variation in the Daihai Lake region of north-central China: a direct indication of the Asian monsoon climatic history. Quat. Sci. Rev. 23, 1669–1679.
Yang, X.D., Wang, S.M., 1996. The vegetational and climatic environmental changes in Hulun Lake and Wulungu Lake during Holocene. Oceanol. Limnol. Sin. 27, 67–72 (in Chinese).
Yang, X.L., Liu, J.B., Liang, F.Y., Yuan, D.X., Yang, Y., Lu, Y.B., Chen, F.H., 2014. Holocene stalagmite $\delta^{18}O$ records in the East Asian monsoon region and their correlation with those in the Indian monsoon region. The Holocene 24, 1657–1664.
Ye, W., 1999. Characteristics of physical environment and conditions of loess formation in Yili area. Xijing. Arid Land Geogr. 22, 9–16 (in Chinese with English abstract).
Yu, W.D., Min, Q.W., Li, X.G., 2002. The features of precipitation in the loess plateau and its possible impacts on vegetation distribution. Resour. Sci. 24, 55–60 (in Chinese with English abstract).
Yu, C.X., Luo, Y.L., Sun, X.J., 2008. A high-resolution pollen records from Hani Lake, Jilin, Northeast China showing climate changes between 13.1 cal. Ka B.P and 4.5 cal. Ka B.P. Qua. Sci. 28, 929–938 (in Chinese with English abstract).
Yuan, D.X., Cheng, H., Edwards, R.L., Dykoski, C.A., Kelly, M.J., Zhang, M.L., Qing, J.M., Lin, Y.S., Wang, Y.J., Wu, J.Y., Dorale, J.A., An, Z.S., Cai, Y.J., 2004. Timing, duration, and transitions of the Last Interglacial Asian Monsoon. Science 304, 575–578.
Zan, J.B., Fang, X.M., Yang, S.L., Nie, J.S., Li, X.Y., 2010. A rock magnetic study of loess from the West Kunlun Mountains. J. Geophys. Res. Solid Earth 115, B10101. https://doi.org/10.1029/2009JB007184.
Zhang, J., Ma, X., Qiang, M., Huang, X., Li, S., Guo, X., Henderson, A.C.G., Holmes, J.A., Chen, F., 2016. Developing inorganic carbon-based radiocarbon chronologies for Holocene lake sediments in arid NW China. Quat. Sci. Rev. 144, 66–82.
Zhao, S., Xia, D., Jin, H., Jia, J., Li, G., Gao, F., Wang, Y., 2016. Long-term weakening of the East Asian summer and winter monsoons during the mid- to late Holocene recorded by aeolian deposits at the eastern edge of the Mu Us Desert. Palaeogeogr. Palaeoclimatol. Palaeoecol. 457, 258–268.